JOURNAL OF CATALYSIS 136, 199–211 (1992)

^{13}C NMR Studies of CO Adsorbed on Supported Rhodium Catalysts: Effects of Alkali Promotion

D. BURTS COMPTON[1] AND THATCHER W. ROOT[2]

Department of Chemical Engineering, University of Wisconsin–Madison, Madison, Wisconsin

Received January 24, 1992; revised March 26, 1992

Changes in the chemical properties of silica-supported Rh catalysts on potassium promotion are observed in the ^{13}C NMR spectra of adsorbed CO. Catalysts prepared by incipient wetness with 2.5% Rh loading and Rh : K ratios of 1 : 0, 3 : 1, and 1 : 3 show relatively constant CO adsorption site character but have large changes in relative populations of linear, bridging, isolated dicarbonyl, and metal-bound CO. Back-bonded metal electrons on CO produce a Gaussian peak near 275 ppm and indicate a transition to metallic behavior of the underlying Rh at high promotion levels. Purely electrostatic effects are shown to be too small to cause the shifts reported for IR and NMR peak positions. Alkali promotion inhibits the breakup of Rh particles and formation of isolated dicarbonyl sites during CO adsorption, probably by the conversion of surface –OH groups to –OK groups.

INTRODUCTION

Many additives are typically included with the active metal in industrial catalyst preparations to alter the catalyst's activity or selectivity (*1*). On Fischer–Tropsch catalysts, alkali salts are added to improve the selectivity to higher hydrocarbons and olefins. The improvement of current catalytic processes depends on the understanding of how these additives can be used to tune catalyst properties. To this end, many techniques have been used to examine how alkali promoters influence the adsorption of CO on transition metals.

Results from studies on both single crystals (*2–9*) and supported metals (*10–12*) have suggested that alkali promoters weaken the C–O bond via electronic interactions mediated by the metal. The deposition of alkali metals onto transition metal crystals generally lowers the metal work function (*2, 3*), decreases the core-level electron binding energies (*3, 13*) and results in increased heat of CO adsorption (*2–8, 13–15*) and reduced C–O stretching frequencies (*4–6, 15*). For those metals on which CO dissociates, alkali metals promote this dissociation (*13, 14*).

One explanation for these promotion effects is the donation of electron density from the alkali promoter into the conduction band of the metal which, in turn, back-donates electron density into the CO $2\pi^*$ antibonding orbital. The increased electron population in the antibonding orbital weakens the C–O bond, as shown by both the increase in CO dissociation and the decrease in C–O stretching frequencies with increased promoter level. Work function and binding energy changes can also be understood in terms of this model. Because the donated electrons are delocalized by the conduction band, these effects are manifested over a long range. Alternatively, some authors (*6, 16*) explain long-range effects as a through-space electrostatic interaction rather than a through-metal backbonding interaction. In this case, the electric field of an adsorbed potassium atom is thought to perturb the

[1] Present address: Eastman Chemical Co., P.O. Box 1972, Kingsport, TN, 37662.

[2] To whom correspondence should be addressed.

0021-9517/92 $5.00

vibrational potential and to shift the stretching frequency of a nearby CO admolecule. Results of vibrational (*2, 6, 18*) and TPD (*4, 7, 17, 19*) studies have also suggested short-range effects due to direct interactions between the alkali and adsorbed CO. Novel CO bonding geometries such as tilted (*19, 20*) or side-on bonded (*2, 15*) species and polymeric CO anion complexes such as oxocarbons (*17*) or etherates (*21*) have been proposed to explain these results.

In most single crystal studies, the alkali is added in elemental form. It is readily ionized, giving up an electron to the underlying transition metal conduction band and achieving a stable inert gas electronic configuration. In supported catalyst systems, where the alkali is typically added as a salt, this model may not be directly applicable. Evaluating this possibility, an XPS study on supported ruthenium catalysts showed that the Ru core-level binding energies do shift upon the addition of alkali salts, and the shifts are similar regardless of the choice of counterion (*22*). Other results on supported catalysts agree with those on single crystals as well (*10–12, 23*), although some have attributed observed selectivities partially or completely to site blockage effects (*23, 24*). An infrared study of CO on K-promoted Rh/SiO_2 catalysts (*12*) found low-frequency stretching peaks near 1800 cm^{-1} that increased in intensity as promoter level was raised. These peaks were attributed to a C–O bond weakened by electronic effects. Another highly promoted catalyst preparation in the same study yielded a strong IR absorption at 1680 cm^{-1} that was attributed to a direct K–CO complex.

There have been several NMR investigations of CO on supported transition metals (*25–37*) but none yet on promoted catalysts. On highly dispersed Rh and Ru catalysts, NMR lineshape analyses (*25*) identify the same linear, bridging, and dicarbonyl bonding structures seen by IR and other techniques. Linear and bridging species are located on metal crystallites and are identified by comparison with spectra of model transition-metal cluster carbonyls. Bridging species resonate near 230 ppm relative to TMS, while linear species resonate upfield at 180 ppm. Bridging and linear lineshapes are also distinguished by different chemical shift anisotropies. Linear species typically absorb over a range of 400 ppm, while bridging species cover only about 200 ppm, and each species has a characteristic asymmetry. Multicarbonyl species can take on several lineshapes depending on their motional properties (*27, 28*). A rigid multicarbonyl is indistinguishable from linear CO on metal particles. The broad resonance line collapses to a narrow Lorentzian centered at the isotropic shift for those species in which the carbonyl groups reorient rapidly and isotropically. A structure has been proposed for this species which involves rotation about two or more nonparallel bonds (*29*) and this species is therefore referred to as a "multirotational" dicarbonyl. A third lineshape has been identified (*27, 28*) on highly dispersed Rh samples characterized by an anisotropy equal to half of the rigid species and inverted through the isotropic shift. This lineshape is due to Rh dicarbonyls with mutually exchanging CO substituents and is referred to as a flipping dicarbonyl.

Spectra of CO on unpromoted Rh, Pd, and Pt catalysts of low dispersion (*29–35*) are very different from those mentioned above. These spectra are instead dominated by Knight-shift interactions caused by the conduction electrons in the larger metallic particles, which mix with the CO molecular orbitals and produce resonances at higher frequencies. This interpretation has been verified for CO on Pt and Pd catalysts in temperature-dependent relaxation studies. The observed Korringa law behavior is a fingerprint for the involvement of conduction electrons in ^{13}C relaxation.

In this paper we report the ^{13}C NMR spectra of CO on silica-supported Rh catalysts modified with different levels of potassium promotion. Spectral features reflect changes in the electronic properties of metal particles as well as changes in surface chemistry

of CO adsorption sites. These changes are generally consistent with the back-donation model. Other reports discuss the use of ^{13}C NMR to examine the effects of different support oxides (*38*) and changes in alkali metal, reduction treatment, and Rh deposition method (*39*).

EXPERIMENTAL METHODS

Silica-supported rhodium catalysts were prepared using incipient wetness to distribute the metal ions in the oxide. The silica used here (Degussa Aerosil 380) has a BET surface area of 270 m^2/g. A 2.5-wt% Rh/silica catalyst was prepared by impregnation of silica to incipient wetness with an aqueous solution of $RhCl_3$ (Aldrich) followed by overnight drying at 373 K. Promoted catalysts were prepared by subsequent incipient-wetness impregnation of the base catalyst with KNO_3 solutions followed by another overnight drying procedure at 363 K. Promoted catalysts were prepared with Rh : K molar ratios of 3 : 1 and 1 : 3.

Catalyst samples were loaded into U-tube reactors described elsewhere (*40*). All catalysts were treated using similar procedures. First, they were heated in flowing helium to 400 K and held there for 1 h. They were then heated in flowing hydrogen to 473 K for 6 h. After reduction, the catalysts were exposed to flowing helium for 1 h, cooled to room temperature in vacuum, and one port of the reactor was sealed. Catalysts were then dosed with several aliquots of 99% ^{13}C-enriched CO (Isotec) at room temperature. Mass spectrometry of the adsorbing gases was used during volumetric uptake to monitor the production of CO_2, and the small amounts of CO_2 produced on these samples during the first few CO doses (<2% of total ^{13}C dosed) were pumped out before beginning subsequent doses. Uptake was slow near saturation, and several days were usually allowed for equilibration. After dosing, the remaining arm of the U-tube was sealed. The sample preparations and ^{13}CO uptake are summarized in Table 1.

^{13}C NMR experiments were performed on a Chemagnetics CMC-300 spectrometer operating at 75.3 MHz. Chemical shifts are plotted on the δ scale, relative to TMS, such that downfield is positive (i.e., C_6H_6 is at 128.7 ppm). Wideline spectra were obtained by Fourier transforming the spin echoes observed after applying a (90°–τ–180°–τ–observe) pulse sequence with τ = 50 μs.Typical 90° pulse times were 4.0 μs. The phases of rf pulses were cycled to minimize receiver mismatch and other artifacts. A spectral width of 250 kHz (3333 ppm) was used to obtain accurate echo spectra and ensure complete detection of all observable carbonaceous species on the catalysts. Spin–spin relaxation times were obtained from spin-echo experiments with a variable echo delay. Spin–lattice relaxation times were obtained from inversion-recovery experiments. At least six inversion delays were used in each case. A recycle delay of 3 s was used for all spectra shown here.

TABLE 1

Descriptions of Silica-Supported Catalysts

Sample	Rh : K	P_{CO} (Torr)[a]	CO : Rh[b]	% Obsd.[c]
RK10IW	1 : 0	11.3	0.87	100[d]
RK31IW	3 : 1	11.2	0.66	97
RK13IW	1 : 3	5.4	0.63	59

[a] Final pressure when sealed (1 Torr = 133.3 N m^{-2}).
[b] Calculated from volumetric uptake. Confidence limits are ±5%.
[c] (^{13}C NMR spin count)/(^{13}CO dosed) × 100%. Confidence limits are ±5%.
[d] Measured value 103% of uptake.

RESULTS

The ^{13}C NMR spectra for the series of catalysts prepared by incipient-wetness are shown in Fig. 1. The centers of mass of the three spectra are 201, 216, and 249 ppm, respectively. All spectra are characterized by a low-frequency tail near −60 ppm. The highest resonance frequency increases from approximately 300 ppm on the unpromoted catalyst to 400 ppm on the highly promoted catalyst.

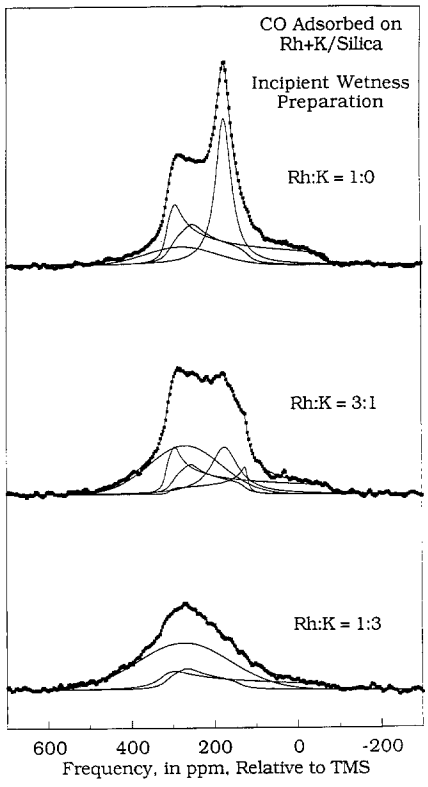

FIG. 1. ^{13}C NMR spectra of CO adsorbed on silica-supported, potassium-promoted Rh catalysts prepared by incipient-wetness impregnation. Spectra of catalysts with Rh : K = 1 : 0, 3 : 1, and 1 : 3 represent the accumulation of 21 000, 28 000, and 35 000 scans, respectively. Parameters for individual subspectra are given in Table 2.

Conspicuous by its absence in the spectra of all of these catalysts is a sharp peak at 124 ppm corresponding to gaseous CO_2. Such a peak was noted in spectra of similar unpromoted Rh and Ru samples (*25*). On those samples, CO_2 was formed during CO adsorption either by oxidation or disproportionation. The small quantity of $^{13}CO_2$ produced during dosing of the samples used here was removed during dosing, and the spectra show that no additional $^{13}CO_2$ was formed.

Attempts were made to fit all spectra with a three-component model, corresponding to CO adsorbed in linear, bridging, and multirotational dicarbonyl sites. The lineshapes initially presumed for these species were (a) a powder pattern centered between 169 and 192 ppm with anisotropy of 260 ± 40 ppm and asymmetry between 0 and 0.15; (b) a powder pattern centered between 220 and 270 ppm with anisotropy of 110 ± 40 ppm and asymmetry between 0.15 and 0.5; and (c) a Lorentzian line centered between 169 and 192 ppm, respectively. These lineshapes agree with those found in ^{13}C NMR studies of similar unpromoted catalysts (*25–27*) and metal carbonyl references compounds (*41*). This three-component model gave adequate agreement with the data only for the unpromoted sample. The potassium-containing samples required a fourth component. The results of several trial lineshapes for this fourth component revealed that the remaining intensity was best fit by a broad Gaussian line centered between 270 and 330 ppm. A four-component model including this Gaussian peak gave improved fits over a model including an extra unconstrained powder pattern. In the spectrum of RK31IW, a flipping dicarbonyl component (*27, 28*) significantly improved the fit to the data. It is characterized by an isotropic shift identical to linearly adsorbed CO with anisotropy of −130 ± 20 ppm and an asymmetry of zero. This species is probably present in all catalyst samples with dicarbonyl populations but was a significant factor only in this spectrum. A summary of the fitted parameters for all samples is presented in Table 2.

Additional parameters will always result in an improvement in the agreement of a model with the data. In order to assess the significance of the extra parameters resulting from the added components given the noise level of the data, we applied the significance tests of Hamilton (*42*). Their application to NMR spectra is straightforward, as described elsewhere (*26*). These tests only give the user a tool to assess the statistical significance of added components and say nothing about whether such components are physically meaningful. Statistical significance is evaluated at the 99.5% confi-

TABLE 2

^{13}C NMR Shielding Parameters for K-Promoted, Silica-Supported Rh Catalysts

Sample	Linear				Bridging				Flipping dicarbonyl			Multirotational dicarbonyl			Metal-bound		
	$\langle\sigma\rangle$	δ	η	area[a]	$\langle\sigma\rangle$	δ	η	area[a]	$\langle\sigma\rangle$	δ	area[a]	$\langle\sigma\rangle$	$\Delta\sigma$	area[a]	$\langle\sigma\rangle$	$\Delta\sigma$	area[a]
RK10IW	183	242	0.09	0.33	224	108	0.50	0.20			[b]	174	23	0.34	277	86	0.13
RK31IW	177	258	0.08	0.25	228	102	0.44	0.13	183	−125	0.08	175	40	0.19	270	87	0.35
RK13IW	188	256	0.01	0.24	242	100	0.50	0.15			[b]			[b]	275	112	0.61

[a] Fractional area.
[b] Inclusion of this species did not significantly improve the fit for this spectrum.

dence level, unless otherwise stated. For the case of the unpromoted catalyst, the addition of the Gaussian peak to the three-component model is judged to be significant. For this catalyst and the Rh : K = 3 : 1 sample, no component is superfluous. For the highly promoted sample, the best four-component model yields zero area for the dicarbonyl CO, so only linear, bridging, and Gaussian peaks are significant.

Both spin–lattice and spin–spin relaxation times were determined for all three catalysts. Spectra obtained from inversion-recovery experiments were fit using the lineshapes derived from the fully relaxed spectra, varying only the areas of each species. The results of these fits for the unpromoted catalyst are shown in Fig. 2. Similar results were obtained for the other catalysts. At the intermediate delays some components have passed through the null point while others remain partially inverted, allowing identification of individual subspectra. Fitting the component intensities to an exponential recovery,

$$M(t) = M_0(1 - 2\xi e^{-t/T_1}),$$

where ξ is the inversion efficiency, yields the T_1 values reported in Table 3. The relaxation curves for the unpromoted sample are shown in Fig. 3. On the promoted samples the T_1's were less disparate, as seen in the table. In all cases, the Gaussian component has a spin–lattice relaxation time distinctly shorter than the other species, confirming its identity as a different species and showing that it has an additional relaxation mechanism.

The spin–spin relaxation times obtained for these components also varied. The magnetization was found to decay exponentially in all cases, but no clear pattern emerged for

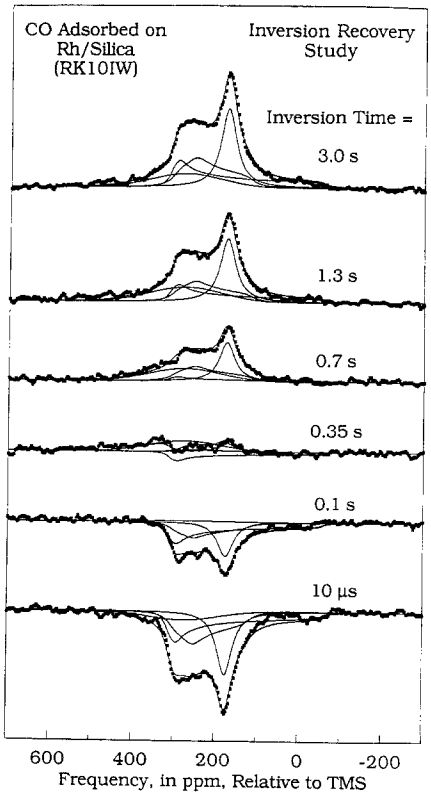

FIG. 2. Inversion-recovery spectra for ^{13}CO adsorbed on silica-supported Rh (sample RK10IW). Delays between inversion and observe pulses are indicated.

TABLE 3

Relaxation Times for Incipient-Wetness Series Catalysts

	Sample	Linear	Bridging	Flipping dicarbonyl	Multirotational dicarbonyl	Metal-bound
T_1 (s)	RK10IW	0.77 ± 0.09	0.43 ± 0.15		0.52 ± 0.08	0.18 ± 0.03
	RK31IW	0.44 ± 0.18	0.32 ± 0.19	0.29 ± 0.06	0.57 ± 0.38	0.23 ± 0.15
	RK13IW	0.51 ± 0.17	0.51 ± 0.30			0.29 ± 0.05
T_2 (ms)	RK10IW	0.64 ± 0.06	0.50 ± 0.13		0.47 ± 0.04	0.18 ± 0.06
	RK31IW	0.57 ± 0.17	0.68 ± 0.45	0.25 ± 0.08	0.52 ± 0.19	0.40 ± 0.05
	RK13IW	0.63 ± 0.17	0.66 ± 0.28			0.62 ± 0.21

the different species. On the highly promoted catalyst, T_2 values were identical within the error limits.

DISCUSSION

Comparison of NMR Results with IR Data

The increase in center-of-mass of the NMR spectrum as promoter level increases is an additional measure of an overall weakening of the C–O bond strength, confirming the weakening indicated by lower stretching frequencies in vibrational studies of CO on promoted catalysts (*2, 6, 10–12, 15, 23, 24*). Recent ab initio calculations of the effects of external electrical perturbations on these two parameters predicted a linear relationship (*43*) with a slope of -0.23 ppm/cm^{-1}. While some curvature is apparent in plots of the ab initio calculations, the results are linear for frequency shifts of up to ± 50 cm^{-1}. Previous study of inorganic carbonyls (*44*) found an inverse correlation for linear carbonyl ligands between the ^{13}C chemical shift and the C–O force constant, which is proportional to the square of the stretching frequency, and this correlation can be used to predict variation of chemical shifts and IR frequencies over limited ranges. On different inorganic carbonyl compound families (*44*), slopes vary from -0.13 to -0.48 ppm/cm^{-1}. This relationship can also be seen for bridge-like carbonyls in several families of organic compounds. C–O stretching frequencies and ^{13}C isotropic shifts for reference compounds, plotted in Fig. 4, show an inverse linear relationship for each series. For the quinones, a slope of -0.68 ppm/cm^{-1} is obtained, while the substituted acetones and haloketones give a slope of -0.57 ppm/cm^{-1}.

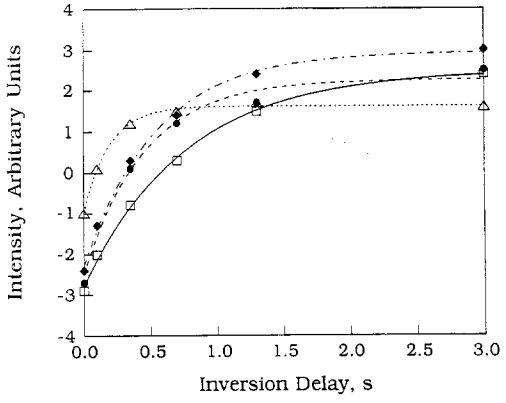

FIG. 3. Inversion-recovery exponential recovery curves for sample RK10IW. (□) Linear, (●) bridging, (◆) dicarbonyl, and (△) metal-bound.

Maciel (*47*) explained the trends in chemical shift of methyl-substituted carbonyl compounds (CH_3COX) by changes in the C–O π-bond polarity. That analysis carefully separated inductive effects due to electron-donating or withdrawing groups from resonance effects due to the keto-enol equilibrium. Back-donation is analogous to the addition of electron-donating groups. Adding such groups results in a more polar C–O bond, which decreases the bond order, force

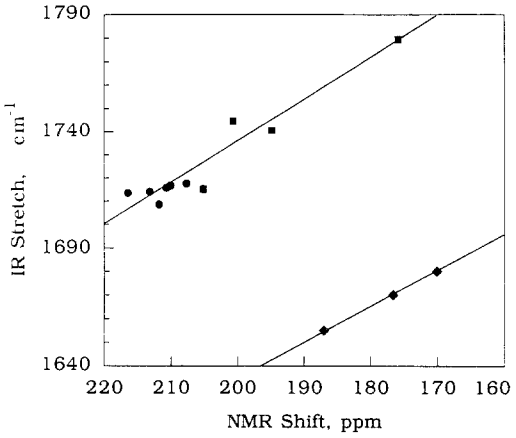

FIG. 4. Comparison of C–O stretching frequencies with ^{13}C chemical shifts for organic carbonyl compound families. Data from Refs. (*45*) and (*46*). (◆) Quinones, (■) halkotenes, and (●) alkyl-substituted acetone.

constant, and stretching frequency and increases the ^{13}C isotropic chemical shift. The observation of a shift in the overall center-of-mass of the NMR lineshape with increased promotion would therefore be predicted by the back-donation model.

While a comparable shift is seen for our samples, this recognition does little to resolve controversies in the mechanism of promotion, as there are several possible explanations for such a shift. The shift in average frequency is caused by changing site populations, while in other catalysts prepared via amine exchange the frequency of each site changes with increasing promoter content (*48*). Conversion of linearly adsorbed CO to a bridging geometry that would shift the resonance to higher frequencies has been proposed (*10*), but is inconsistent with the site populations measured here. Other studies (*2–6, 12–17, 19, 21, 23, 24*) have attributed promotion effects to the formation of new sites, distinguished by an interaction between CO and the alkali—either directly or mediated through the metal. Our results support this new-site explanation and also provide a means for quantifying the affected sites. These new sites are manifested in our spectra as Gaussian components seen here, located at frequencies higher than those found for linear and bridging CO of model carbonyl compounds. It is the growing intensity of this species that accounts for much of the increased center-of-mass of the NMR lineshape with increased alkali content.

This Gaussian peak at 275 ppm appears at high-promotion conditions. Vibrational studies show a new peak at or below 1800 cm^{-1} on supported Rh (*12*), Rh(111) (*4*), Ni(111) (*6*), and Pt(111) (*8*) at high alkali loadings. This new species has been characterized as a localized species, and ionic complexes such as $K_x^{\delta+}(CO)_y^{\delta-}$ of the oxocarbon (*17*) or etherate (*21*) form were suggested based on vibrational spectra. However, NMR spectra of representative stable oxocarbons, including $K_2(CO)_4$, $K_2(CO)_5$, and $K_2(CO)_6$, show that they all have isotropic shifts of 175–210 ppm (*48*). Unless $K_2(CO)_2$ has very different behavior, polymeric oxocarbon-like $K_x^{\delta+}(CO)_y^{\delta-}$ complexes are not a good model for this new surface species. No NMR data for the proposed etherate structure is presently available, and the effects of K^+ and Rh neighbors are difficult to predict. However, organic ethers typically have isotropic shifts of 50–100 ppm and small (50–80 ppm) anisotropies (*49*). No such species were detected with NMR on these supported catalyst samples containing Rh : K ratios up to 1 : 3. Unfortunately, neither NMR nor vibrational studies can determine if a promoted K–CO complex has a definite stoichiometry. While NMR spin counts give the quantity of CO in the Gaussian peak, the actual K coverage on the Rh particles is unobtainable, and IR or HREELS studies on single crystals can work with known K coverages but cannot usually determine CO concentrations directly from vibrational spectra.

The NMR results from the promoted catalyst series can be more closely compared with IR results from similar catalysts studied by Kesraoui *et al.* (*12*). There, a highly promoted (Rh : K = 1 : 5) catalyst showed no absorption due to dicarbonyls or bridging

CO, but did contain peaks in the linear range and at 1808 cm^{-1}. Our results also indicate the presence of linear sites and absence of dicarbonyls on a highly promoted (Rh : K = 1 : 3) sample. In contrast with the IR results, the NMR spectrum indicates 15% of all adsorbed CO to be in bridging sites. The most prominent feature in the infrared spectrum is a broad band at 1808 cm^{-1} that increases in intensity with increased promotion. This frequency is below that of typical bridge-bonded CO and was attributed to a new species modified by electronic interactions with the promoter (*12*). The appearance of this new low-frequency IR peak corresponds to the increase in intensity of the Gaussian lineshape in the NMR spectra. If the 1808 cm^{-1}, 275 ppm species is a modified linear site, an NMR shift/IR shift slope of -0.36 ppm/cm^{-1} can be calculated, while if it is a modified bridged site, as seems more likely (*12*), a slope of -0.49 ppm/cm^{-1} results. Both values are somewhat higher than predicted from the ab initio calculations and lower than the organic compounds, but within the range of those seen on metal cluster carbonyls.

Estimation of Through-Space Effects

Opposite trends in the ^{13}C chemical shift and the stretching frequency of CO can also be caused by strictly external electrical perturbations, such as electric fields or field gradients. Ab initio calculations of Augspurger *et al.* (*43*) provide a means of quantitatively determining the effects of various electric potentials on these parameters. The measured shifts are seen to depend strongly on the angle between the applied field or field gradient and the CO internuclear axis. To ascertain the magnitude of a through-space electrostatic interaction for our catalysts, we have calculated the field and field gradient due to the alkali promoter species next to an adsorbed CO molecule. A simple model was used by Uram *et al.* (*6*) to qualitatively explain the decrease in CO stretching frequency on potassium coadsorption on an Ni(111) surface. This model treats the alkali ion as a point charge located above an infinite conducting plane. The electric field at a nearby CO admolecule is calculated as the vector sum of that due to the K^+ ion and its image charge. We investigated the effect using a similar geometry with some modifications.

We assumed a potassium radius of 2.12 Å, the equilibrium distance calculated for a K atom outside a jellium surface (*16*). Carbon and oxygen positions were those obtained in LEED analysis of CO on Rh(111) (*50*). The lateral distance between K^+ and ^{13}CO center-of-mass at closest approach was approximated as the sum of the Rh–C distance and the effective K radius. Following Augspurger *et al.* (*43*), the angle θ between the field or field gradient and the C–O axis is defined as 0° for a field oriented from oxygen to carbon.

The electric field due to a point charge is given by

$$E = \frac{1}{4\pi\varepsilon_0}\frac{q}{r^2},$$

and the field gradient is

$$EFG = -\frac{\partial E}{\partial r} = \frac{2}{4\pi\varepsilon_0}\frac{q}{r^3}.$$

Both E and EFG are oriented radially away from a positive charge and towards a negative charge. The electric field is 0.0167 a.u. (1 a.u. = 5.142 25 × 10^9 V/cm) with θ = 21.4° and the field gradient is 0.00520 a.u. (1 a.u. = 9.717 45 × 10^{17} V/cm^2) with θ = 13.2° for the effect of K^+ and its image charge. The contour plots of Augspurger *et al.* predict frequency shifts of +9 ppm and -45 cm^{-1} due to the field and +2 ppm and +12 cm^{-1} due to the field gradient, for an overall ^{13}C NMR shift of +11 ppm and an overall change in the CO stretching frequency of -33 cm^{-1}.

The above model does not account for the metallic screening of the potential. Lang *et al.* (*16*) have included this effect in calculations of the electrostatic potential due to adsorbed alkalis. Using their contour maps of the induced electrostatic potential due to

an adsorbed K atom with the geometry of the previous model, the calculated electric field is 0.0051 a.u. with $\theta = 39°$. This contributes only +3 ppm to the ^{13}C chemical shift and decreases the CO stretching frequency by only 15 cm^{-1}. Even if the 1808 cm^{-1}, 275 ppm species is the least shifted, modified bridge structure described above, by either approach we can conclude that the through-space electrostatic effects are insufficient to cause the ~45 ppm increase in ^{13}C shift seen for the Gaussian component of these spectra and the corresponding ~92 cm^{-1} decrease in CO stretching frequency.

Interpretation of Gaussian Peak

The NMR spectrum of ^{13}CO on the highly promoted catalyst does not have the definition seen in the less highly promoted samples. Lacking information from other spectroscopies, one would be tempted to fit this spectrum to a simple Gaussian or Lorentzian lineshape. However, the infrared results discussed above clearly indicate the presence of linear CO, and omitting this component also significantly decreases the quality of the fit to the NMR spectrum.

Similar featureless peaks have been noted on unpromoted rhodium catalysts of low dispersion (*29*). It is unlikely, however, that the results here indicate simply an increase in particle size. Measurements of particle size using X-ray line-broadening have shown a decrease in particle size on alkali promotion (*12*). The decreased CO : Rh ratios with promotion seen here therefore reflect the blockage of available adsorption sites by the promoter and the prevention of dicarbonyl site formation, rather than a true decrease in the Rh dispersion.

Another species that would resonate at 300–400 ppm is a surface carbide, as might be formed during CO hydrogenation by coking or CO dissociation. However, IR data (*12*) show a 1808 cm^{-1} C–O stretch appearing at comparable alkali loading, so the new CO species has not dissociated. In addition, EELS spectra on alkali-promoted Rh(111) surfaces (*4*) show no M–C or M–O stretching modes. Finally, a carbonaceous overlayer (*40*) does not exhibit the short T_1 seen here, so the surface carbide possibility can be ruled out.

It has been proposed that the transition from multiple powder patterns to a single broad peak corresponds to the onset of metallic behavior in supported metal particles (*29*). Metallic (as opposed to diamagnetic) particles possess a nonzero magnetic susceptibility that can affect the spectra of adsorbed species. The effect of the magnetic susceptibility can be calculated for any standard geometry. For linear CO on a spherical particle, the anisotropy is decreased by $8\pi\chi/3$, or 112 ppm for Rh (*30*). Calculation for bridging CO requires unavailable knowledge of the principle axis system, but will generally result in decreased anisotropy and increased asymmetry. Of course, particles are not strictly spherical, with larger clusters approaching a regular polyhedral geometry (*30*). For such clusters, the value of the magnetic susceptibility may change from site to site, leading to additional broadening. Magnetic susceptibility depends on particle size (*51, 52*) which may further broaden the NMR lineshape. In addition, χ varies with adsorbate and coverage (*51*). Thus the presence of potassium salts on the promoted catalysts may serve to alter the magnetic susceptibility and lead to further broadening. The broadening due to the site distribution may substantially increase the linewidth from the theoretical prediction. It is not surprising then that the present Gaussian peaks have halfwidths of 200–250 ppm, while that seen for unpromoted catalysts of low dispersion is only 90 ppm (*29*).

The magnetic susceptibility interaction has no isotropic part and therefore can only broaden or narrow the lineshape; it cannot shift the center-of-mass. This interaction cannot be responsible for the high frequency of the Gaussian peak. Such a frequency shift must be caused by either a chemical shift or a Knight shift. A chemical shift due to a direct interaction with the promoter salt is

unlikely, as compounds containing potassium are rarely shifted greatly from their organic analogues. For example, the isotropic shift of the carbonyl carbon of acetic acid is 188 ppm, while that of potassium acetate is 177 ppm (*49*), a shift of only 11 ppm and in the opposite direction to that observed here. Additional chemical shift may be caused by electron-donating substituents, as described above, but the shifts shown in Fig. 4 are significantly smaller than those seen for this new peak. The range of shifts seen for the Gaussian peaks on the different promoted catalysts also extends above the range of shifts commonly seen for CO in model inorganic carbonyl clusters (*41*) although there is some slight overlap. We conclude that the high frequency of the Gaussian peak is most likely caused by a Knight shift, which occurs because the Rh conduction electrons influence the magnetic field at the ^{13}C nucleus.

Knight shifts have been implicated in the high shifts seen on Pd, Pt, Os, and Ir (*30–35*) and temperature-dependent relaxation studies have proven this to be the operating mechanism for Pd and Pt (*31, 32*). NMR of ^{13}CO on Pd/SiO_2 or Pd/Al_2O_3 catalysts show the isotropic frequency of Knight-shifted CO on Pd (760 ppm) to be far from that of normal chemically shifted CO (190 ppm). Intensity at 190 ppm was assigned to linear CO adsorbed at edges and corners of metal particles, while the remaining intensity was attributed to bridging CO adsorbed on Pd faces (*35*). The Knight-shifted bridging CO resonates over a wide range of shifts between these two extremes, and is not appreciably narrowed in a TOSS experiment. With only a moderate particle-size distribution, as determined from electron microscopy measurements described in that study, this range is seen to reflect heterogeneity in the bridged bonding sites and the extent of overlap between the CO molecular orbitals and the conduction band of the Pd. Similar Knight-shifted CO adsorbed on 30–150 Å colloidal Pd particles has been detected indirectly (*53*).

The shifts seen for ^{13}CO on other supported Group VIII metals, including Rh (*25, 26, 30, 36*), are in the range of chemical shifts for model inorganic carbonyls (*41*) and show no Knight shift. However, the particles in these catalysts may be too small to have a developed conduction band and therefore may be unable to produce a Knight shift. Indeed, on the larger particles of a low-dispersion Rh catalyst the Lorentzian line for CO was centered at 270 ppm (*29*). While this is at the end of the range of bridging CO chemical shifts, it is downfield of the center of mass of the spectra of CO on more highly dispersed catalysts. Since the change in dispersion will not dramatically change the bonding geometry of bridging CO, the increase in center of mass can be interpreted as a Knight shift.

The inversion-recovery data support the Knight-shift interpretation. These experiments show that metal-bound CO relaxes faster than bridging and linear CO. Spin–lattice relaxation can be broken down into contributions from the contact, orbital, and dipolar terms of the hyperfine interaction (*33*). The contribution of the contact term via s-state or σ-orbital electrons can be calculated from the magnitude of the Knight shift using the Korringa relation (*54*). Since

$$T_1K^2 = \frac{\kappa}{4\pi k_B T}\left(\frac{\gamma_e}{\gamma_n}\right)^2 B,$$

where B is a function of electron–electron couplings that is of order unity, $T_1K^2 \approx 1.4 \times 10^4$ s for ^{13}C at room temperature (*33, 54*). Here, K is the Knight shift expressed in ppm. The observed relaxation rate ($1/T_1$) will be the sum of relaxation due to all mechanisms. Considering either Knight-shifted linear or bridging CO to cause the 275 ppm peak, the shifts of 100 or 45 ppm produce Knight-shift relaxation times of 1.4 and 6.9 s. Using average spin–lattice relaxation times for the linear and bridged sites (0.57 and 0.42 s) to describe effects of all other relaxation mechanisms, we predict a relaxation time of 0.4 s for either modified

metal-bound species. This is longer than the values of 0.18–0.29 s actually observed, and so the contact contribution alone is not sufficient to explain the lower relaxation time measured for the metal-bound species. However, as shown by Ansermet *et al.* (*33*), the orbital and dipolar terms of the hyperfine interaction also contribute significantly to the relaxation of a metal-bound species. These terms will be most affected by a change in the back-bonding, as they depend on both the π and σ molecular orbitals, while the contact term depends only on σ-bonding. Thus, the small value of the Knight shift shows an increase in Rh–CO σ-bonding on promoted catalysts, while the additional increase in the relaxation rate also indicates an increase in the Rh–CO π-backbonding.

To summarize, the transition from diamagnetic metal clusters to metallic particles is indicated by the loss of spectral character due to magnetic susceptibility effects and the shift to higher frequency due to a Knight shift. Both the ^{13}C Knight shift and the additional increase in ^{13}C relaxation rate indicate metal electrons are present on the CO. The fraction of CO on metallic particles rises with increasing promoter levels, in agreement with the back-donation model. As promoter is added, more electrons are donated to the metal conduction band and smaller particles begin to exhibit metallic behavior. The increase in the fraction of Knight-shifted CO is quantitatively seen in the increased fractional area of the metal-bound peak.

Rh sites of low coordination, such as at edges and corners of particles, may account for the relatively unperturbed linear CO lineshape seen on promoted catalysts. The CO adsorbed there is not Knight-shifted even on highly promoted catalysts. These Rh atoms may retain diamagnetic behavior because of their low orbital overlap with the developing conduction band of the particle, and are often described as electron-deficient (*35*). Alternatively, their behavior may reflect a limited range for the promoter interaction. The effective range of the promoter electronic perturbation cannot be determined from these NMR spectra. However, since both NMR and IR show that bridging CO is converted to the promoted species at high potassium levels, it appears that the faces of the Rh particles are modified by the potassium promotion. The remaining unpromoted linear CO sites would then be only at the particle edges or corners.

The decrease in CO adsorption on the promoted catalysts may be caused by alkali located on the Rh, leaving fewer Rh sites open. However, significant CO chemisorption occurs on Rh particles even at Rh : K = 1 : 3, in contrast to behavior seen for catalysts with similar composition prepared by amine exchange (*48*).

Role of K in CO-Induced Restructuring of Rh

Results on these catalysts clearly show a monotonic decrease in the fractional area of the dicarbonyl as promoter level increases. Although infrared results on a similar catalyst series (*12*) show an initial increase in the amount of adsorbed dicarbonyl on a low-promotion sample, they mention that this result is anomalous. The dicarbonyl species is absent on a highly promoted sample, in agreement with results here. Two alternatives can be offered to explain this decrease in dicarbonyl formation. Either the potassium prevents the dicarbonyl from forming or it increases the rate of reductive agglomeration of the isolated Rh^I sites to form Rh_x^0 particles. Both explanations have been supported by infrared studies. Solymosi *et al.* (*55*) found that Rh dicarbonyl vibrational bands decrease more rapidly on K_2O-doped Al_2O_3 than on a similar undoped catalyst at 448 K. The authors attributed the observed differences to an electronic effect. Little difference was noted in the two samples at room temperature, however. Zaki *et al.* (*56*) showed that K_2CO_3 will react with relatively basic Al–OH groups on Al_2O_3 to form Al–OK groups, which block the oxidative disruption of Rh_x^0 crystallites by CO. This

reaction is activated. Although some hydroxyls were replaced upon heat treatment at 570 K, most of the reaction occurred when the Al_2O_3–K_2CO_3 was heated at 770 K. Infrared spectroscopy indicated that the most basic and nucleophilic OH groups were replaced most easily (*57*). Hydroxyl groups of silica are more basic than those of alumina and should therefore be more susceptible to attack from the electropositive promoter. Our results indicate that a similar mechanism operates on our catalysts, and the 6 h reduction treatment at 473 K is sufficient to replace many of the Si–OH groups with Si–OK groups. This prevents formation of isolated Rh^I sites on adsorption of CO.

The NMR spin counts from spectra of the unpromoted and moderately promoted samples show all adsorbed CO has been detected (Table 1). The decrease in observed CO at high promoter levels cannot be due to a paramagnetic dicarbonyl species, since IR spectra (*12*) show that there is no dicarbonyl CO present at high K loadings. The promoter species must therefore render some of the CO located on the metal particles unobservable.

CONCLUSIONS

An increase in center-of-mass of the ^{13}C NMR spectra of CO adsorbed on silica-supported Rh catalysts with increased alkali promotion demonstrates a weakening of the C–O bond. This overall shift is due largely to the growing contribution of a Gaussian line located downfield from normal chemically shifted CO. The appearance and intensity of this line corresponds with low-frequency vibrational peaks reported in infrared spectra of similar catalysts. Electrostatic effects alone cannot explain the large shifts seen for these species in both NMR and IR spectroscopies. The Gaussian peak is interpreted as a species in which metal conduction electrons mix with the CO molecular orbitals. This assignment is supported by the observation of similar peaks on Rh catalysts of lower dispersion and catalysts of metals with higher magnetic susceptibility. This species relaxes more rapidly than CO on nonmetallic particles, as expected with the involvement of conduction electrons in d–π Rh–CO back bonding. Such an interpretation is significant in that it supports the existence of the through-metal electronic interaction that has been debated in the surface science literature, although NMR results do not indicate the effective range of this interaction. While prior vibrational studies have found evidence for oxocarbon or etherate complexes, the ^{13}C NMR spectra of the samples investigated here have no features corresponding to these complexes.

In addition to affecting the CO on metal particles, alkali promoters also block the formation of dicarbonyl sites on isolated Rh atoms by exchanging with surface hydroxyl groups during catalyst preparation and forming unreactive –OK groups. The formation of these isolated sites is something to be avoided, as they are catalytically inactive for CO hydrogenation or dissociation, so this prevention of CO-induced Rh redispersion is another useful effect of alkali promotion.

ACKNOWLEDGMENTS

Support for this research was provided by National Science Foundation Grant CBT-8657496, the AT&T Foundation, and the Shell Oil Foundation. We also thank Dr. Robert Weber for helpful discussions.

REFERENCES

1. Dry, M. E., *Appl. Ind. Catal.* **2,** 167 (1983).
2. de Paola, R. A., Hrbek, J., and Hoffmann, F. M., *J. Chem. Phys.* **82,** 2484 (1985).
3. Kiskinova, M., Pirug, G., and Bonzel, H. P., *Surf. Sci.* **133,** 321 (1983).
4. Crowell, J. E., and Somorjai, G. A., *Appl. Surf. Sci.* **19,** 73 (1984); Crowell, J. E., Tysoe, W. T., and Somorjai, G. A., *J. Phys. Chem.* **89,** 1598 (1985).
5. Sun, Y.-M., Luftman, H. S., and White, J. M., *J. Vac. Sci. Technol. A* **2,** 883 (1984).
6. Uram, K. J., Ng, L., Folman, M., and Yates, J. T., Jr., *J. Chem. Phys.* **84,** 2891 (1986); Uram, K. J., Ng, L., and Yates, J. T., Jr., *Surf. Sci.* **177,** 253 (1986).
7. Lee, J., Arias, J., Hanrahan, C. P., Martin, R. M., and Metiu, H., *J. Chem. Phys.* **82,** 485 (1985).

8. Crowell, J. E., Garfunkel, E. L., and Somorjai, G. A., *Surf. Sci.* **121,** 303 (1982).
9. Ishi, S.-I., Ohno, Y., and Viswanathan, B., *J. Sci. Ind. Res.* **46,** 541 (1987).
10. Gonzalez, R. D., and Miura, H., *J. Catal.* **77,** 338 (1982).
11. Okuhara, T., Tamura, H., and Misono, M., *J. Catal.* **95,** 41 (1985).
12. Kesraoui, S., Oukaci, R., and Blackmond, D. G., *J. Catal.* **105,** 432 (1987).
13. Broden, G., Gafner, G., and Bonzel, H. P., *Surf. Sci.* **84,** 295 (1979).
14. Benziger, J., and Madix, R. J., *Surf. Sci.* **94,** 119 (1980).
15. Hoffmann, F. M., and de Paola, R. A., *Phys. Rev. Lett.* **52,** 1697 (1984).
16. Lang, N. D., Holloway, S., and Norskov, J. K., *Surf. Sci.* **150,** 24 (1985).
17. Lackey, D., Surman, M., Jacobs, S., Grider, D., and King, D. A., *Surf. Sci.* **152/153,** 513 (1985).
18. Angevaare, P. A. J. M., Hendrickx, H. A. C. M., and Ponec, V., *J. Catal.* **110,** 18 (1988).
19. Netzer, F. P., Doering, D. L., and Madey, T. E., *Surf. Sci.* **143,** L363 (1984).
20. Kiskinova, M., Szabo, A., and Yates, J. T., Jr., *Surf. Sci.* **205,** 215 (1988).
21. Sinniah, K., Sands, W. D., Yates, J. T., Jr., and Janda, K. C., *J. Am. Chem. Soc.* **113,** 3684 (1991).
22. Shyu, J. Z., Goodwin, J. G., Jr., and Hercules, D. M., *J. Phys. Chem.* **89,** 4983 (1985).
23. McClory, M. M., and Gonzalez, R. D., *J. Catal.* **89,** 392 (1984).
24. Blackmond, D. G., Williams, J. A., Kesraoui, S., and Blazewick, D. S., *J. Catal.* **101,** 496 (1986).
25. Duncan, T. M., and Root, T. W., *J. Phys. Chem.***92,** 4426 (1988).
26. Duncan, T. M., Zilm, K. W., Hamilton, D. M., and Root, T. W., *J. Phys. Chem.* **93,** 2583 (1989).
27. Thayer, A. M., and Duncan, T. M., *J. Phys. Chem.* **93,** 6763 (1989).
28. Molitor, P., and Apple, T., *J. Phys. Chem.* **93,** 7055 (1989).
29. Duncan, T. M., *Colloids Surf.* **45,** 11 (1990).
30. Slichter, C. P., *Annu. Rev. Phys. Chem.* **37,** 25 (1986).
31. Shore, S. E., Ansermet, J.-P., Slichter, C. P., and Sinfelt, J. H., *Phys. Rev. Lett.* **58,** 953 (1987).
32. Rudaz, S. L., Ansermet, J.-P., Wang, P.-K., Slichter, C. P., and Sinfelt, J. H., *Phys. Rev. Lett.* **54,** 71 (1985).
33. Ansermet, J.-P., Wang, P.-K., Slichter, C. P., and Sinfelt, J. H., *Phys. Rev. B* **37,** 1417 (1988).
34. Zilm, K. W., Bonneviot, L., Hamilton, D. M., Webb, G. G., and Haller, G. L., *J. Phys. Chem.***94,** 1463 (1990).
35. Zilm, K. W., Bonneviot, L., Haller, G. L., Han, O. H., and Kermarec, M., *J. Phys. Chem.* **94,** 8495 (1990).
36. Duncan, T. M., Yates, J. T., Jr., and Vaughan, R. W., *J. Chem. Phys.* **73,** 975 (1980).
37. Thayer, A. M., Duncan, T. M., and Douglass, D. C., *J. Phys. Chem.* **94,** 2014 (1990).
38. Compton, D. B., and Root, T. W., submitted for publication.
39. Compton, D. B., and Root, T. W., submitted for publication.
40. Duncan, T. M., Winslow, P., and Bell, A. T., *J. Catal.* **93,** 1 (1985).
41. Gleeson, J. W., Vaughan, R. W., *J. Chem. Phys.* **78,** 5384 (1983).
42. Hamilton, W. C., *Acta Crystallogr.* **18,** 502 (1965).
43. Augspurger, J. D., Dykstra, C. E., and Oldfield, E., *J. Am. Chem. Soc.* **113,** 2447 (1991).
44. Mann, B. E., *J. Chem. Soc., Dalton Trans.*, 2012 (1973).
45. "The Sadtler Standard Spectra." Sadtler Research Laboratories, Philadelphia, PA, 1965.
46. Levy, G. C., Lichter, R. L., and Nelson, G. L., "Carbon-13 Nuclear Magnetic Resonance Spectroscopy." Wiley, New York, 1980.
47. Maciel, G. E., *J. Chem. Phys.* **42,** 2746 (1964).
48. Compton, D. B., and Root, T. W., unpublished work.
49. Duncan, T. M., "A Compilation of Chemical Shift Anisotropies." Farragut Press, Chicago, IL, 1990; *J. Phys. Chem. Ref. Data* **16,** 125 (1987).
50. Van Hove, M. A., Koestner, R. J., Frost, J. C., and Somorjai, G. A., *Surf. Sci.* **129,** 482 (1983).
51. Halperin, W. P., *Rev. Mod. Phys.* **58,** 533 (1986).
52. Candy, J. P., and Perrichon, V., *J. Catal.* **89,** 93 (1984).
53. Bradley, J. S., Millar, J. M., Hill, E. W., *J. Am. Chem. Soc.* **113,** 4016 (1991).
54. Slichter, C. P., "Principles of Magnetic Resonance." Springer-Verlag, Berlin, 1990.
55. Solymosi, F., Pasztor, M., and Rakhely, G., *J. Catal.* **110,** 413 (1988).
56. Zaki, M. I., Ballinger, T. H., and Yates, J. T., Jr., *J. Phys. Chem.* **95,** 4028 (1991).
57. Kantschewa, M., Albano, E. V., Ertl, G., and Knozinger, H., *Appl. Catal.* **8,** 85 (1983).